JACS
JOURNAL OF THE AMERICAN CHEMICAL SOCIETY
Article
pubs.acs.org/JACS

Entrapping a Group-VB Transition Metal, Vanadium, within an Endohedral Metallofullerene: $V_xSc_{3-x}N@I_h$-C_{80} (x = 1, 2)

Tao Wei,[†] Song Wang,[†] Xing Lu,[‡] Yuanzhi Tan,[§] Jing Huang,[∥] Fupin Liu,[†] Qunxiang Li,[∥] Suyuan Xie,[§] and Shangfeng Yang*[,†]

[†]Hefei National Laboratory for Physical Sciences at Microscale, Key Laboratory of Materials for Energy Conversion, Chinese Academy of Sciences, Department of Materials Science and Engineering, Synergetic Innovation Center of Quantum Information & Quantum Physics, University of Science and Technology of China (USTC), Hefei 230026, China

[‡]State Key Laboratory of Materials Processing and Die & Mold Technology, College of Materials Science and Engineering, Huazhong University of Science and Technology (HUST), Wuhan 430074, China

[§]State Key Laboratory of Physical Chemistry of Solid Surfaces and Department of Chemistry, College of Chemistry and Chemical Engineering, Xiamen University, Xiamen 361005, China

[∥]Hefei National Laboratory for Physical Sciences at Microscale & Department of Chemical Physics, University of Science and Technology of China (USTC), Hefei 230026, China

Supporting Information

ABSTRACT: So far the entrapped metals for the isolated endohedral metallofullerenes (EMFs) are primarily limited to rare earth metals, whereas except group-IVB metals, whether it is possible to entrap other d-block transition metals remains unclear. Herein we report the successful entrapment of the group-VB transition metal vanadium(V) into fullerene cage, affording the heretofore unknown V-containing EMFs. Two novel V-containing EMFs—$V_xSc_{3-x}N@C_{80}$ (x = 1, 2)—were isolated, and their molecular structures were unambiguously determined by X-ray crystallography to be $I_h(7)$-C_{80} cage entrapping the planar VSc_2N/V_2ScN clusters. $V_xSc_{3-x}N@I_h(7)$-C_{80} (x = 1, 2) were further characterized by UV−vis−NIR and ESR spectroscopies and electrochemistry, revealing that the electronic and magnetic properties of $V_xSc_{3-x}N@I_h(7)$-C_{80} (x = 1, 2) are tunable upon varying the number of entrapped V atoms (i.e., x value). The molecular structures and electronic properties of $V_xSc_{3-x}N@I_h(7)$-C_{80} (x = 1, 2) were further compared with those of the reported analogous EMFs based on lanthanide metals and the adjacent group-IVB transition metal Ti, revealing the peculiarity of the group-VB transition metal V-based EMFs.

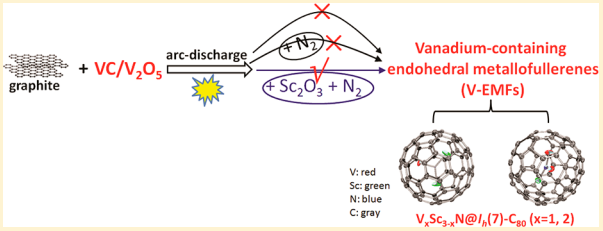

INTRODUCTION

One of the unique and fascinating structural characteristics of fullerenes is that its interior is spherically hollow, and this naturally leads to the inspiration to entrap atoms into the carbon cage so as to tailor the molecular and electronic properties of fullerenes.[1,2] Endohedral metallofullerenes (EMFs) thus formed represent a special form of carbon nanostructures, with atoms, ions or clusters entrapped in the interior of fullerene cage.[1−9] Many fascinating properties of EMFs have been demonstrated as the result of the charge transfer and electrostatic interactions between the entrapped metal(s) and the carbon cage.[1−10] The entrapment of metal(s) within EMFs also brings about versatile potential applications of EMFs in the fields such as electronics, biomedicine, photovoltaics, and materials science, for which EMFs usually show superior performance than empty fullerenes, and in some cases the applications are only accessible for EMFs owing to the contribution of the entrapped metal.[1,3,9] As the first stable EMF, $La@C_{82}$ was isolated by Smalley et al. in 1991, for which a three-electron transfer from La to the C_{82} cage occurs, leading to an electronic configuration of $La^{3+}@C_{82}^{3-}$.[11] Later on, many other metals have been entrapped in EMFs in different forms such as conventional (metal-only) EMFs,[12] including mono-metallofullerenes, dimetallofullerenes and trimetallofullerenes, and clusterfullerenes[8] in which an unstable metal cluster is entrapped, and considerable advance has been achieved in the field of EMFs during the past two decades.[1−9] Nevertheless, so far the entrapped metals of the isolated EMFs are quite limited, based primarily on rare earth metals including Group-IIIB (Sc, Y) and lanthanide metals.[1,3] Besides, a few main-group metals including group-IIA (Ca, Sr, Ba),[13,14] group-IA (Li, Na, K)[15,16] and group-IVB transition metals (Ti, Zr, Hf)[17−19] have been also reported to form EMFs. In particular, for a large number of d-block transition metals except group-IIIB and group-IVB ones, it is yet unclear whether or not they could be entrapped into carbon cage to form EMFs. In specific, to our knowledge, vanadium(V)-containing EMFs have never been reported

Received: September 26, 2015
Published: December 8, 2015

DOI: 10.1021/jacs.5b10115
J. Am. Chem. Soc. 2016, 138, 207−214

despite that V element is just next to titanium (Ti) in the first (3d) transition metal series. Since the properties of EMFs are dependent on the entrapped metal, entrapping new metal (especially those in group-VB and beyond) into carbon cage is highly important and desirable for extending the potential applications of EMFs, which is however quite challenging.

Herein, we report the successful entrapment of a group-VB transition metal, vanadium(V), into fullerene cage, affording the heretofore unknown V-containing EMFs. The formation of both conventional EMFs and clusterfullerenes containing V is investigated, and two novel V-containing EMFs—$V_xSc_{3-x}N@C_{80}$ (x = 1, 2)—were isolated, whose molecular structures including the cage isomeric structures and the geometries of the entrapped $V_xSc_{3-x}N$ clusters were unambiguously determined by X-ray crystallography. $V_xSc_{3-x}N@C_{80}$ (x = 1, 2) were further characterized by various spectroscopic methods and electrochemistry, revealing that the electronic and magnetic properties of $V_xSc_{3-x}N@C_{80}$ (x = 1, 2) are tunable upon varying the number of entrapped V atoms. By comparing the molecular structures and electronic properties of $V_xSc_{3-x}N@C_{80}$ (x = 1, 2) with those of the reported analogous EMFs based on the lanthanide metals and the adjacent group-IVB transition metal Ti, the peculiarity of the V-based EMFs is unveiled.

RESULTS AND DISCUSSION

Synthesis and Isolation of V-Containing EMFs. It is well-known that the production yield of EMFs especially metal nitride clusterfullerenes (NCFs) is strongly dependent on the size of the entrapped metal ion.[1,7,8,20] Vanadium(V) has variable positive oxidation states from +2 to +5 with the ionic radius being 0.46, 0.58, 0.64, and 0.79 Å for V^{5+}, V^{4+}, V^{3+} and V^{2+}, respectively, which is, except V^{2+}, much smaller than those of group-IIIB metals (e.g., 0.75 Å for Sc^{3+} as the smallest one).[21] The relatively smaller size of V ion stimulates us to investigate the possibility of entrapping V into fullerene cage in different forms including the conventional (metal-only) EMFs and clusterfullerenes.[1,8,12] As the first and intuitive attempt, we attempted to synthesize V-containing conventional EMFs. In this study we chose two common and commercially available V sources with different oxidation states of V, i.e., V_2O_5 and VC, which was mixed with graphite and subject to Krätschmer-Huffman DC-arc discharging under 400 mbar He. To detect the composition of the fullerene extract, laser desorption time-of-flight mass spectroscopic (LD-TOF MS) analysis was carried out. According to a comparative analysis of the HPLC profiles of fullerene extracts obtained by using V_2O_5 (or VC) mixed with graphite or pure graphite as starting materials, clearly the profiles of V_2O_5 (or VC) extracts show no discernible difference to that of empty fullerene extract, suggesting that no V-containing conventional EMF forms under this condition, as confirmed further by LD-TOF MS analysis (Supporting Information Figures S1(I) and S2).

Since the discovery of $Sc_3N@C_{80}$ in 1999 fulfilled by introducing a small portion of nitrogen gas into the Krätschmer–Huffman generator,[22] metal nitride clusterfullerenes (NCFs) as a new class of EMFs have been receiving great attentions due to their high yield, peculiar structures and physiochemical properties.[1,7,8,20] Thus, we next made attempts to synthesize V-containing NCFs ($V_3N@C_{2n}$) by using a modified Krätschmer–Huffman DC-arc discharging method with the addition of ~5% N_2. However, the HPLC combined with LD-TOF MS analysis revealed that the composition of fullerene extracts obtained by using VC with N_2 addition was almost identical to that of VC without N_2 addition (Supporting Information Figures S1(I) and S2). This suggests that, despite of the smaller ionic radius of V^{3+} (0.64 Å) compared to that of Sc^{3+} (0.75 Å),[21] no V-containing NCFs ($V_3N@C_{2n}$) forms under this condition either.

Among NCFs, mixed metal nitride clusterfullerenes (MMNCFs) represent a special branch of NCFs with the advantages of not only boosting the yield over the homogeneous NCFs but also behaving as a matrix to induce the entrapment of another metal which is often difficult to be entrapped to form homogeneous NCFs.[23] Utilizing such a exclusive MMNCF-based strategy, previously we successfully entrapped group-IVB metal Ti into the fullerene cage and isolated two Ti-based MMNCFs $TiM_2N@C_{80}$ (M = Sc, Y).[18,24,25] This encouraged us to use the MMNCF-based strategy to synthesize V-containing EMF in the present work. VC (or V_2O_5) was mixed with Sc_2O_3 and graphite at an optimized molar ratio of 1:1:15 (V:Sc:C) and used for DC-arc discharging under the addition of ~5% N_2. Interestingly, the HPLC profiles of the VC/Sc_2O_3/N_2 and V_2O_5/Sc_2O_3/N_2 extracts are almost identical (Supporting Information Figure S1(II)), suggesting that the oxidation state of V in the starting V source hardly affect the formation of fullerenes. Thus, in the following discussions we take VC/Sc_2O_3/N_2 extract only as an example.

The HPLC profile of the VC/Sc_2O_3/N_2 extract is compared with those of the VC/N_2 and Sc_2O_3/N_2 extracts, revealing a subtle difference for the major fraction **A** (t_{ret} = 46.9–49.9 min), which is obviously split into a major subfraction **A2** (t_{ret} = 48.1–49.9 min) and a shoulder subfraction **A1** (t_{ret} = 46.9–48.1 min) for the VC/Sc_2O_3/N_2 extract (see inset of Figure S1II). Since the change of fraction **A** is observed in VC/Sc_2O_3/N_2 extract only, the mixing effect of VC and Sc_2O_3 should be responsible for the splitting of fraction **A**, which must originate from the variation of composition due to either the change of the relative abundance of the existing components or the formation of new components. According to LD-TOF MS analysis of fraction **A** isolated from different extracts, there are two new mass peaks at m/z = 1115 and 1121 detected exclusively in subfraction **A1** of VC/S_2O_3/N_2 extract. Since subfraction **A1** does not exist in Sc_2O_3/N_2 extract, the new mass peaks at m/z = 1115 and 1121 observed in VC/Sc_2O_3/N_2 extract may be due to the formation of V-containing EMFs (Supporting Information Figure S3).

By using three-step HPLC (see Supporting Information Figure S4 for the detailed isolation procedure), in this work we successfully isolated two novel V-containing EMFs —$V_xSc_{3-x}N@I_h(7)$-C_{80} (x = 1, 2, ~15 and 2.5 mg (~99% purity) obtained from 200 g of soot products, respectively). Shown in Figure 1 is the LD-TOF MS spectra of the two subfractions **A-3−1** and **A-3−2**, showing a single mass peak at m/z = 1121 and 1115 corresponding to $V_2ScN@C_{80}$ and $VSc_2N@C_{80}$ MMNCFs, respectively. The chemical identification of the isolated new components, i.e., $VSc_2N@C_{80}$ and $V_2ScN@C_{80}$, is further accomplished by the isotopic distribution analysis of their mass peaks at 1115 and 1121 which shows a good coincidence with the calculated one (see insets of Figure 1). The relative yield of $V_2ScN@I_h(7)$-C_{80}:$VSc_2N@I_h(7)$-C_{80}:$Sc_3N@I_h(7)$-C_{80} is estimated to be 1:6.8:308.8 according to the integrated area of the corresponding peak in HPLC (Supporting Information S4). Such a quite low yield of $V_2ScN@I_h(7)$-C_{80} and $VSc_2N@I_h(7)$-C_{80} relative to that of

DOI: 10.1021/jacs.5b10115
J. Am. Chem. Soc. 2016, 138, 207–214

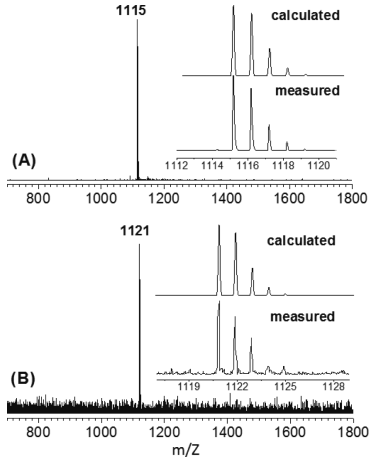

Figure 1. Positive-ion laser desorption time-of-flight (LD-TOF) mass spectra of $VSc_2N@C_{80}$ (A) and $V_2ScN@C_{80}$ (B) corresponding to the isolated fraction **A-3−2** and **A-3−1**, respectively. The insets show the measured and calculated isotope distributions of $VSc_2N@C_{80}$ and $V_2ScN@C_{80}$.

$Sc_3N@I_h(7)$-C_{80} makes their isolation very tedious. On the other hand, the lower yield of $V_2ScN@I_h(7)$-C_{80} than that of $VSc_2N@I_h(7)$-C_{80} follows the tendency of the reported lanthanide metal-based MMNCFs $M_xSc_{3-x}N@I_h(7)$-C_{80} (M = Y, Nd, Gd, Dy, Er, Lu) for which $M_2ScN@C_{80}$ has a lower yield than that of $MSc_2N@C_{80}$,[26−30] while the estimated relative yield of $V_2ScN@I_h(7)$-C_{80}:$VSc_2N@I_h(7)$-C_{80} (1:6.8) is even lower than that of lanthanide metal-based $M_xSc_{3-x}N@I_h(7)$-C_{80} MMNCFs (e.g., $Gd_2ScN@I_h(7)$-C_{80}:$GdSc_2N@I_h(7)$-C_{80} = 1:3.9).[28]

For the reported lanthanide metal-based MMNCFs, there are generally not only $I_h(7)$-C_{80} but also $D_{5h}(6)$-C_{80} isomers, such as $M_xSc_{3-x}N@C_{80}$ (M = Gd, Ho, Dy, Lu).[27−30] However, for the $TiSc_2N@C_{80}$ MMNCF based on group-IVB transition metal Ti we reported previously, only $I_h(7)$ isomer of $TiSc_2N@C_{80}$ was isolated and $TiSc_2N@D_{5h}(6)$-C_{80} was not detected likely due to its lower stability than that of $TiSc_2N@I_h(7)$-C_{80}.[18] Therefore, it is intriguing to address whether $D_{5h}(6)$-C_{80} isomers of $V_xSc_{3-x}N@C_{80}$ exist or not. Interestingly, according to our preliminary results, $V_xSc_{3-x}N@D_{5h}(6)$-C_{80} isomers did exist for both $V_2ScN@C_{80}$ and $VSc_2N@C_{80}$ despite of their even lower yield than those of $V_xSc_{3-x}N@I_h(7)$-C_{80} isomers, and their isolations were underway in our lab. Therefore, the peculiarity of the group-VB transition metal V-based EMFs compared to that based on the adjacent group-IVB transition metal Ti is revealed.

Molecular Structures of $V_xSc_{3-x}N@C_{80}$ (x = 1, 2) Determined by X-ray Crystallography. High-quality black cocrystals of $V_xSc_{3-x}N@C_{80}$ (x = 1, 2) with Ni^{II}(OEP) (OEP = octaethylporphyrin) with the chemical forms of $VSc_2N@C_{80}$·Ni^{II}(OEP)·1.67C_6H_6·0.33$CHCl_3$ and $V_2ScN@C_{80}$·Ni^{II}(OEP)·2C_6H_6 were obtained and used for X-ray crystallographic study,[31−38] affording the unambiguous determination of their molecular structures as $V_xSc_{3-x}N@I_h(7)$-C_{80} (x = 1, 2). Figure 2 shows the relative orientations of $VSc_2N@I_h(7)$-C_{80}/$V_2ScN@I_h(7)$-C_{80} and the Ni^{II}(OEP) molecules in $VSc_2N@C_{80}$·Ni^{II}(OEP)·1.67C_6H_6·0.33$CHCl_3$/ $V_2ScN@C_{80}$·Ni^{II}(OEP)·2C_6H_6, in which only one orientation of the fullerene cage together with the major site of VSc_2N/V_2ScN cluster was shown in the drawing for clarity. Similar to the case of the majority of cocrystals composed of NCFs and

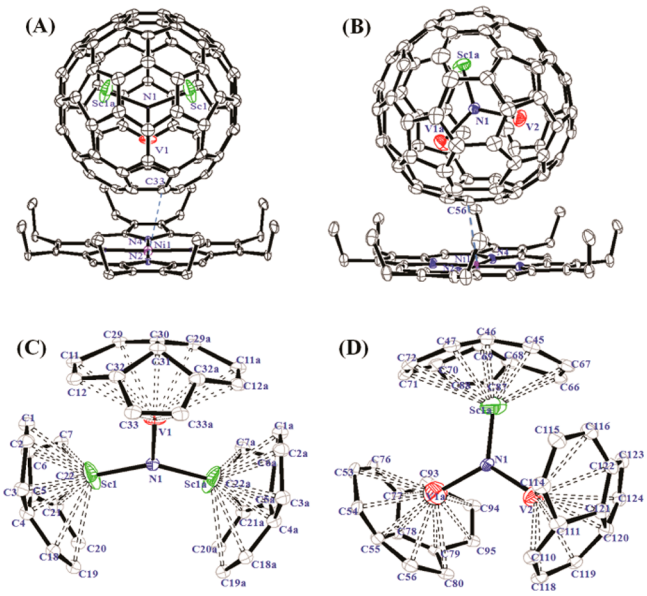

Figure 2. Drawings of the crystallographically determined structures of $V_xSc_{3-x}N@C_{80}$ (x = 1, 2) along with their relation to the Ni^{II}(OEP) molecule and positions of the major $V_xSc_{3-x}N$ cluster site with respect to the nearest carbon atoms of the $I_h(7)$-C_{80} cage. (A, C) $VSc_2N@I_h(7)$-C_{80} with the major C_{80} cage (0.409 occupancy) and the most abundant VSc_2N location (0.601 occupancy); (B, D) $V_2ScN@I_h(7)$-C_{80} with the major C_{80} cage (0.376 occupancy) and one of the V_2ScN location. Thermal ellipsoids are set at 30% probability level. Solvent molecules, the minor cage and minor metal positions are omitted for clarity. Red: V; Green: Sc; Blue: N; Gray: C; Purple: Ni.

Ni^{II}(OEP),[31,37,38] these two cocrystals are both monoclinic with a space group of $C2/m$. Thus, their asymmetric unit cells both contain a half of the Ni^{II}(OEP) molecule and a half of $VSc_2N@C_{80}/V_2ScN@C_{80}$ molecule (see Supporting Information S6 for detailed discussions on their crystallographic structures).

The positions of metal atoms within the fullerene cage of EMFs provide valuable information on the metal (cluster)−cage interactions.[1−3,7,8] For the major sites of both $I_h(7)$-C_{80} cage and the internal VSc_2N cluster within $VSc_2N@I_h(7)$-C_{80}, V atom and two Sc atoms are all located at the junctions of one pentagon and two hexagons (see Figure 2C). This case resembles that of $ErSc_2N@I_h(7)$-C_{80}[39] but is obviously different to those of the reported lanthanide metal-based MMNCFs $MSc_2N@I_h(7)$-C_{80} (M = La, Ce, Gd, Tb) for which the larger metal atom (La, Ce, Gd, Tb) resides under the centers of hexagons while the smaller Sc atoms are located at the intersection of hexagons and pentagons.[40−42] Similar to the cases of V/Sc atoms within $VSc_2N@I_h(7)$-C_{80}, within $V_2ScN@I_h(7)$-C_{80} the two V atoms and one Sc atom also lie at the junctions of one pentagon and two hexagons (see Figure 2D). The difference on the locations of the entrapped metals within $VSc_2N@I_h(7)$-C_{80} and $V_2ScN@I_h(7)$-C_{80} compared with those within $MSc_2N@I_h(7)$-C_{80} (M = La, Ce, Gd, Tb) suggests their different cluster-cage interactions resulted from their discrepancy of the ionic radius of metal. Besides, the position of entrapped V atom within VSc_2N/V_2ScN cluster relative to the Ni^{II}(OEP) molecule is contrary to those of the lanthanide metals within the lanthanide metal-based MMNCFs $MSc_2N@C_{80}$ (M = La, Ce, Gd, Tb, Er) and $Gd_2ScN@I_h(7)$-C_{80}, in which the large lanthanide metal atom M located in the site furthest away from the Ni^{II}(OEP).[39−42] Instead, within

DOI: 10.1021/jacs.5b10115
J. Am. Chem. Soc. 2016, 138, 207−214

$VSc_2N@I_h(7)$-C_{80}/$V_2ScN@I_h(7)$-C_{80} the V atom(s) is situated near the Ni^{II}(OEP), whereas the Sc atom(s) locates far away from the Ni^{II}(OEP) molecule. This is however understandable because the ionic radius of V^{3+} (0.64 Å) is smaller than that of Sc^{3+} (0.75 Å), whereas within MSc_2N (M = La, Ce, Gd, Tb, Er) or Gd_2ScN cluster the M^{3+} is generally much larger than Sc^{3+}, as a result the positions of V and Sc ions are both reversed relative to those within $MSc_2N@C_{80}$ (M = La, Ce, Gd, Tb, Er) and $Gd_2ScN@I_h(7)$-C_{80}.[39−42] These results indicate the structural peculiarity of the group-VB transition metal V-based MMNCFs compared to those based on the reported lanthanide metals.

For NCFs including MMNCFs the geometric configuration of the entrapped cluster is sensitively dependent on the size of the internal metal ion, and a planar configuration of small Sc_3N cluster within $Sc_3N@I_h(7)$-C_{80} would change to a pyramidal one for a relatively larger Gd_3N cluster within $Gd_3N@I_h(7)$-C_{80}.[22,43] It is hence of interest to investigate the geometric configuration of the entrapped VSc_2N/V_2ScN cluster. For the major site of VSc_2N cluster, the Sc1(Sc1a)−N1−V1 and Sc1−N1−Sc1a angles is 112.1(3)° and 134.6 (5)°, respectively, and the sum of these three angles about the central nitrogen atom is 358.8°, which is quite close to that of $Sc_3N@I_h(7)$-C_{80} (358.38°).[44] Thus, the four-atomic VSc_2N cluster is planar with a C_{2v} symmetry. Likewise, the sum of Sc1a−N1−V1a (119.46(17)°), Sc1a−N1−V2 (120.0(3)°) and V1a−N1−V2 (120.5(3)°) angles is 359.96° for one site of V_2ScN clusters (see Supplemental Table S4), indicating that the entrapped V_2ScN cluster is planar as well. These results are easily understood because the ionic radius of V^{3+} (0.64 Å) is even smaller than that of Sc^{3+} (0.75 Å)[21] thus a planar VSc_2N/V_2ScN cluster is preferred.

For the major site of VSc_2N cluster within $VSc_2N@I_h(7)$-C_{80}, the Sc1(Sc1a)-N1 and V1−N1 bond distance is 2.036(4) Å and 1.858(7) Å, respectively. Interestingly, the Sc−N bond distance within VSc_2N cluster is obviously larger than those reported for other lanthanide metal-based MMNCFs such as $LaSc_2N@I_h(7)$-C_{80} (1.943(6) Å, 1.921(7) Å), $CeSc_2N@I_h(7)$-C_{80} (1.942(2) Å, 1.933(2) Å), $GdSc_2N@I_h(7)$-C_{80} (1.916(9) Å, 1.919(8) Å), $TbSc_2N@I_h(7)$-C_{80} (1.949(8) Å) and $ErSc_2N@I_h(7)$-C_{80} (1.986(6) Å) as well as $Sc_3N@I_h(7)$-C_{80} (1.9931(14) Å, 2.0323(16) Å, 2.0526(14) Å).[39−42,44] A plausible explanation is that the involvement of V^{3+} with much smaller ionic radius than those of lanthanide metal ions may lead to the elongation of the Sc−N bond. Similarly, the Sc−N bond distance in V_2ScN cluster is 2.003(6) Å, which is still larger than that in $Gd_2ScN@C_{80}$ (1.911(3) Å).[40] Noteworthy, with a further substitution of Sc by V ion, the Sc−N bond distance within V_2ScN cluster slightly decreases compared to that within VSc_2N cluster (2.036(4) Å) and becomes more close to that within $Sc_3N@I_h(7)$-C_{80} (1.9931(14) Å, 2.0323(16) Å, 2.0526(14) Å).[44] Such a shortening of the Sc−N bond distance in V_2ScN moiety results in an elongation of V−N bond distance (1.995(5) Å, 2.027(3) Å) compared with that within VSc_2N cluster (1.858(7) Å). The crystallographic structure data of $VSc_2N@I_h(7)$-C_{80} and $V_2ScN@I_h(7)$-C_{80} are summarized in Supplemental Table S4, which includes also those of $MSc_2N@I_h(7)$-C_{80} (M = La, Ce, Gd, Tb, Er), $Gd_2ScN@I_h(7)$-C_{80} and $Sc_3N@I_h(7)$-C_{80} for comparison.[39−42,44]

Spectroscopic Studies on the Electronic Properties of $V_xSc_{3-x}N@I_h(7)$-C_{80} (x = 1, 2). The electronic properties of $V_xSc_{3-x}N@I_h(7)$-C_{80} (x = 1, 2) were studied by UV−vis−NIR and electron spin resonance (ESR) spectroscopy (Supporting Information S7−S9). The UV−vis−NIR spectra of $V_xSc_{3-x}N@I_h(7)$-C_{80} (x = 1, 2) dissolved in toluene are shown in Figure 3,

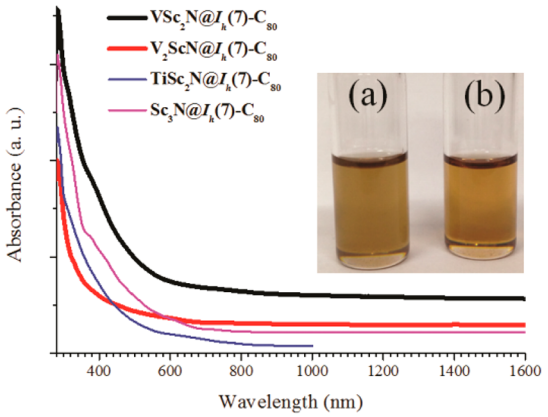

Figure 3. UV−vis−NIR spectra of $VSc_2N@I_h(7)$-C_{80} and $V_2ScN@I_h(7)$-C_{80} dissolved in toluene in comparison with those of $TiSc_2N@I_h(7)$-C_{80} and $Sc_3N@I_h(7)$-C_{80}. Insets: the photographs of $VSc_2N@I_h(7)$-C_{80} (a) and $V_2ScN@I_h(7)$-C_{80} (b) in toluene.

which includes also those of $Sc_3N@I_h(7)$-C_{80} and $TiSc_2N@I_h(7)$-C_{80}[18] for comparison, and their characteristic absorption data is summarized in Tables 1 and S5. In overall the electronic absorption spectra of $V_xSc_{3-x}N@I_h(7)$-C_{80} (x = 1, 2) are less rich in features than that of $Sc_3N@I_h(7)$-C_{80} with no sharp absorption peak detected (see Supporting Information S7 for detailed analysis of the absorption peaks), and this feature is similar to $TiSc_2N@I_h(7)$-C_{80}.[18] The higher resemblance of $V_2ScN@I_h(7)$-C_{80} instead of $VSc_2N@I_h(7)$-C_{80} to $TiSc_2N@I_h(7)$-C_{80} is somewhat unexpected because the number of substituted Sc atom (i.e., x value of $M_xSc_{3-x}N@C_{80}$) is quite different for $V_2ScN@C_{80}$ and $TiSc_2N@C_{80}$. Moreover, on the basis of the absorption spectral onset of ca. 1700 and 1290 nm (Supporting Information Figure S7), the optical band-gaps of $VSc_2N@I_h(7)$-C_{80} and $V_2ScN@I_h(7)$-C_{80} are estimated to be ca. 0.73 and 0.96 eV (see Table 1), respectively, which are both much smaller than those of $Sc_3N@I_h(7)$-C_{80} (1.51 eV) and $TiSc_2N@I_h(7)$-C_{80} (1.43 eV).[18,22] As a result, the colors of $VSc_2N@I_h(7)$-C_{80} and $V_2ScN@I_h(7)$-C_{80} in toluene are both brown-yellow. These results indicate the dramatic influence of the electronic structure of $Sc_3N@I_h(7)$-C_{80} upon the substitution of Sc with V atom. Compared to $V_2ScN@I_h(7)$-C_{80}, again unexpectedly there is obviously a much larger deviation of $VSc_2N@I_h(7)$-C_{80} to $TiSc_2N@I_h(7)$-C_{80} and $Sc_3N@I_h(7)$-C_{80}, suggesting that the substitution of one Sc with one V atom in $VSc_2N@C_{80}$ results in an even larger influence than the case of two Sc atoms' substitution in $V_2ScN@C_{80}$. Thus, the electronic properties of $V_xSc_{3-x}N@C_{80}$ (x = 1, 2) are tunable upon varying the number of entrapped V atoms (i.e., x value).

For the previously reported lanthanide metal-based MMNCFs $M_xSc_{3-x}N@I_h(7)$-C_{80} (M = Y,[26] Ce,[42] Nd,[27] Gd,[28] Tb,[40] Dy,[29] Ho,[30] Er,[39] Lu[27]), the electronic absorption spectroscopic results revealed that, with the change of composition of the entrapped $M_xSc_{3-x}N$ cluster (i.e., x value), the absorption spectra $M_xSc_{3-x}N@I_h(7)$-C_{80} generally exhibit small changes in terms of a slight increase of the optical band gap (<0.1 eV) and the development of a more resolved absorption pattern with the increase of the number of lanthanide metal M in the cluster.[26−30] This tendency seems

DOI: 10.1021/jacs.5b10115
J. Am. Chem. Soc. 2016, 138, 207−214

Table 1. Redox Potentials (V vs Fc^+/Fc), Electrochemical Gaps ($\Delta E_{gap,ec}$) and Optical Band-Gaps ($\Delta E_{gap,optical}$) of $V_xSc_{3-x}N@I_h(7)$-C_{80} (x = 1, 2) in Comparison with Those of $TiSc_2N@I_h(7)$-C_{80} and $Sc_3N@I_h(7)$-C_{80}

	$E_{1/2}$ (V vs Fc/Fc^+)										
	reduction steps (E_{red})					oxidation step (E_{ox})					
sample	first	second	third	fourth	fifth	first	second	$\Delta E_{gap,EC}$/V[a]	absorption onset (λ_{onset}, nm)	$\Delta E_{gap,optical}$/eV[b]	ref.
$VSc_2N@I_h(7)$-C_{80}	−0.42	−0.66	−1.33	−1.71	−2.32[c]	0.44[c]	–	0.86	1700	0.73	this work
$V_2ScN@I_h(7)$-C_{80}	−0.77[c]	−2.38	–	–	–	0.60	1.07[c]	1.37	1290	0.96	this work
$TiSc_2N@I_h(7)$-C_{80}	−0.94	−1.58	−2.21	–	–	0.16	–	1.10	870	1.43	18
$Sc_3N@I_h(7)$-C_{80}	−1.29[c]	−1.56[c]	–	–	–	0.59	–	1.88	820	1.51	6, 30

[a] $\Delta E_{gap,EC} = E_{1/2,ox(1)} - E_{1/2,red(1)}$. [b] $\Delta E_{gap,optical} = 1240/\lambda_{onset}$. [c] E_p: peak potential.

not applicable for the present $V_xSc_{3-x}N@I_h(7)$-C_{80} (x = 1, 2) since the difference on the optical band-gaps of $VSc_2N@I_h(7)$-C_{80} and $V_2ScN@I_h(7)$-C_{80} reaches 0.23 eV. This indicates that, although V atom can substitute Sc atom to form two variable nitride clusters of $V_xSc_{3-x}N$ (x = 1, 2) like the lanthanide metal, its influence on the electronic property of $V_xSc_{3-x}N@C_{80}$ is quite different to that of lanthanide metal. Thus, the peculiarity of the electronic property of group-VB transition metal V-based EMFs is revealed.

An ionic model of $[(M^{3+})_3N^{3-}]^{6+}@C_{80}^{6-}$ based on a formal transfer of six electrons from the entrapped metal nitride to the outer carb on cage has been confirmed for NCFs including a wealth of $M_xSc_{3-x}N@C_{80}$ MMNCFs.[10,26−30,39−44] Thus, a similar electronic configuration of $\{[(V^{3+})_x(Sc^{3+})_{3-x}]N^{3-}\}^{6+}@C_{80}^{6-}$ is anticipated for $V_xSc_{3-x}N@C_{80}$ (x = 1, 2) with the entrapped V ion taking a formal valence state of +3. The electronic configurations of V and Sc atoms are $[Ar]3d^34s^2$ and $[Ar]3d^14s^2$, respectively. When V takes a formal valence state of +3, two unpaired electrons are expected to be localized on V^{3+} ($3d^2$), suggesting that both $VSc_2N@C_{80}$ and $V_2ScN@C_{80}$ would be paramagnetic. This suggestion was experimentally confirmed by the lack of ^{13}C NMR signal after the spectrum accumulation for 24 h and further by the detection of the evident ESR signals at 130 K for both $VSc_2N@C_{80}$ and $V_2ScN@C_{80}$, showing broad signals with the g-factor of 1.9998 and 2.1998 for $VSc_2N@C_{80}$ and $V_2ScN@C_{80}$, respectively (Supporting Information Figure S8). In addition to the smaller g-factor of $VSc_2N@C_{80}$ than that of $V_2ScN@C_{80}$, the line width of the ESR signal of $VSc_2N@C_{80}$ (36 G) is also much smaller than that of $V_2ScN@C_{80}$ (72 G), indicating that the magnetic properties of $V_xSc_{3-x}N@C_{80}$ (x = 1, 2) are tunable upon varying the number of entrapped V atoms (i.e., x value). Interestingly, the severe broadening of the ESR signal of $V_xSc_{3-x}N@C_{80}$ (x = 1, 2) is similar to the cases of $TiM_2N@C_{80}$ (M = Sc, Y) reported previously,[18,24,25] and this seems to be a common feature for transition metal-containing MMNCFs while further variable-temperature ESR measurements are needed to unveil the mechanism responsible for such a broadening of the ESR signal.[24] In order to understand the reason for their discrepancy on the ESR signal, we performed DFT calculation at GGA-PBE/DNP level to compute the spin density of these two entrapped clusters, and found that the spin density was mainly located on the V^{3+} ion(s) for both VSc_2N and V_2ScN clusters (see Supporting Information S9 for detailed analysis of the DFT calculated spin density). Hence, the smaller g-factor and line width of the ESR signal of $VSc_2N@C_{80}$ than those of $V_2ScN@C_{80}$ may probably be due to the entrapment of one more paramagnetic V^{3+} ion within $V_2ScN@C_{80}$.

Electrochemical Study of $V_xSc_{3-x}N@I_h(7)$-C_{80} (x = 1, 2). Figure 4 presents cyclic voltammograms of $VSc_2N@I_h(7)$-C_{80} and $V_2ScN@I_h(7)$-C_{80} measured in o-dichlorobenzene (o-DCB) with tetrabutylammonium hexafluorophosphate ($TBAPF_6$) as supporting electrolyte. The characteristic redox potentials are summarized in Table 1, which includes also those of $TiSc_2N@I_h(7)$-C_{80} and $Sc_3N@I_h(7)$-C_{80} for comparison.[18] In the anodic region, $VSc_2N@I_h(7)$-C_{80} exhibits one electrochemically irreversible oxidation step with a peak potential (E_p) at 0.44 V, and this is completely different to that of $TiSc_2N@I_h(7)$-C_{80} which shows one reversible oxidation step with half wave potential ($E_{1/2}$) at 0.16 V.[18] In addition to the positive shift of the first oxidation potential, the irreversible oxidation behavior has been scarcely reported for rare earth

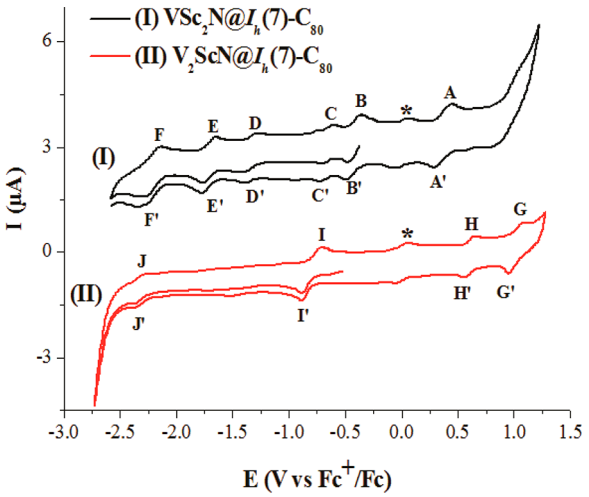

Figure 4. Cyclic voltammograms of $VSc_2N@I_h(7)$-C_{80} and $V_2ScN@I_h(7)$-C_{80} in o-DCB solution with ferrocene (Fc) as the internal standard under different scan regions. Scan rate: 100 mV/s, $TBAPF_6$ as supporting electrolyte. (I) $VSc_2N@I_h(7)$-C_{80}: **B**, **C**, **D**, **E**, **F** label the first to fifth reduction peaks, and the corresponding reoxidation peaks are **B′**, **C′**, **D′**, **E′**, **F′**, respectively. **A** and **A′** mark the oxidation peak and its corresponding rereduction peaks. (II) $V_2ScN@I_h(7)$-C_{80}: **I** and **J** label the first and second reduction peaks, and the corresponding reoxidation peaks are **I′**, **J′**, respectively. **H** and **G** mark the first and second oxidation peak, and the corresponding reoxidation peaks are **H′**, **G′**. The asterisks label the oxidation peak of ferrocene. Both curves are shifted vertically for clarity.

DOI: 10.1021/jacs.5b10115
J. Am. Chem. Soc. 2016, 138, 207−214

metal-based NCFs including MMNCFs,[1,6−8,20] suggesting once more the peculiarity of EMFs based on the group-VB metal V compared to those based on the commonly studied rare earth metals and group-IVB metal Ti. On the other hand, in the cathodic region, $VSc_2N@I_h(7)$-C_{80} shows a complex and more unique feature with up to five reduction steps observed under the common electrochemical window and room temperature. The first four reduction steps are evidently reversible and $E_{1/2}$ is observed at −0.42, −0.66, −1.33, and −1.71 V, respectively, while the fifth reduction step turns into irreversible with E_p being at −2.32 V (Supporting Information Figure S10a). Again, such a reduction behavior of $VSc_2N@I_h(7)$-C_{80} is dramatically different to that of $TiSc_2N@I_h(7)$-C_{80} which shows only three reversible reduction steps,[18] all being negatively shifted compared to those of $VSc_2N@I_h(7)$-C_{80}. Such a big difference between these two non-group-IIIB metal-based MMNCFs $MSc_2N@I_h(7)$-C_{80} (M = V, Ti) reveals the strong influence of the entrapped metal (V or Ti) on the electronic property of $MSc_2N@C_{80}$. The more positive reduction potentials of $VSc_2N@I_h(7)$-C_{80} than $TiSc_2N@I_h(7)$-C_{80} suggests that $VSc_2N@I_h(7)$-C_{80} has a stronger electron-accepting ability. By comparing the overall redox behavior of $MSc_2N@I_h(7)$-C_{80} (M = V,Ti), we hypothesized that the peculiarity of the electrochemical property of $VSc_2N@I_h(7)$-C_{80} may result from one more unpaired electron located on the 3d orbital of V^{3+} ion.

For $V_2ScN@I_h(7)$-C_{80}, two oxidation steps were clearly observed: the first oxidation step is reversible with $E_{1/2}$ at 0.60 V, which is positively shifted relative to that of $VSc_2N@I_h(7)$-C_{80}, and the second oxidation step appears irreversible with E_p at 1.07 V. In the cathodic region, surprisingly only two reduction steps were detected for $V_2ScN@I_h(7)$-C_{80}: the first one is irreversible with E_p at −0.77 V, whereas the second one is reversible with $E_{1/2}$ at −2.38 V (Supporting Information Figure S10b). This abrupt reduction feature leads to a very large separation (1.61 V) between the first and second reduction steps, which has never been observed in the reported rare earth metal-based NCFs including MMNCFs.[1,6−8,20] This unprecedented finding provides further evidence on the peculiarity of the group-VB metal V-based EMFs compared to those based on the commonly studied rare earth metals. Resulted from the distinct discrepancy on both the oxidation and reduction steps, $VSc_2N@I_h(7)$-C_{80} and $V_2ScN@I_h(7)$-C_{80} show quite different electrochemical gap ($\Delta E_{gap,ec}$), which is 0.86 and 1.37 V, respectively (see Table 1). Noteworthy, the fact that the electrochemical gap of $VSc_2N@I_h(7)$-C_{80} is much smaller than that of $V_2ScN@I_h(7)$-C_{80} agrees well with their difference on the optical band gap obtained from the above UV−vis−NIR characterization. All of these distinct discrepancies on the redox property between $V_2ScN@I_h(7)$-C_{80} and $VSc_2N@I_h(7)$-C_{80} confirm further that the electronic properties of $V_xSc_{3-x}N@C_{80}$ (x = 1, 2) are tunable upon varying the number of entrapped V atoms (i.e., x value), and this provides a facile route to tailor the applications of EMFs in electronics, photovoltaics and so forth.

CONCLUSION

In summary, the heretofore unknown V-containing EMFs, $V_xSc_{3-x}N@C_{80}$ (x = 1, 2), have been successfully synthesized and isolated, opening the access to group-VB transition metal by fullerene for the first time. The molecular structures of $V_xSc_{3-x}N@C_{80}$ (x = 1, 2) were unambiguously determined by X-ray crystallography to be $I_h(7)$-C_{80} cage entrapping the planar VSc_2N/V_2ScN clusters. UV−vis−NIR and ESR spectroscopic characterizations combined with electrochemical study reveal that the electronic and magnetic properties of $V_xSc_{3-x}N@I_h(7)$-C_{80} (x = 1, 2) are tunable upon varying the number of entrapped V atoms (i.e., x value). By comparing the molecular structures and electronic properties of $V_xSc_{3-x}N@I_h(7)$-C_{80} (x = 1, 2) with those of the reported analogous EMFs based on lanthanide metals and the adjacent group-IVB transition metal Ti, the peculiarity of the group-VB transition metal V-based EMFs is unveiled, including (1) contrary to the cases of the lanthanide metal-based MMNCFs $MSc_2N@C_{80}$ (M = La, Ce, Gd, Tb, Er) and $Gd_2ScN@I_h(7)$-C_{80} in which the large lanthanide metal atom M located in the site furthest away from the Ni^{II}(OEP), within $VSc_2N@I_h(7)$-C_{80}/$V_2ScN@I_h(7)$-C_{80} the V atom(s) is situated near the Ni^{II}(OEP), whereas the Sc atom(s) locates far away from the Ni^{II}(OEP) molecule; (2) the substitution of one Sc with one V atom in $VSc_2N@I_h(7)$-C_{80} results in a larger deviation of the electronic property to those of $TiSc_2N@I_h(7)$-C_{80} and $Sc_3N@I_h(7)$-C_{80} than the case of two Sc atoms' substitution in $V_2ScN@I_h(7)$-C_{80}; (3) $VSc_2N@I_h(7)$-C_{80} exhibits the irreversible oxidation behavior which has been scarcely reported for rare earth metal-based NCFs including MMNCFs, and $V_2ScN@I_h(7)$-C_{80} has only two reduction steps with a very large separation (1.61 V), which has never been observed in the reported rare earth metal-based NCFs. Our success on the first entrapment of the group-VB transition metal V within fullerene cage represents a breakthrough for fullerene research, and is highly expected to stimulate exploration for novel EMFs containing alternative group-VB metals or beyond toward extended applications in catalysis and photovoltaics, etc.

EXPERIMENTAL METHODS

Synthesis and Isolation of $V_xSc_{3-x}N@C_{80}$ (x = 1, 2). By using a mixture of VC (or V_2O_5), Sc_2O_3, and graphite powder with a molar ratio of 1:1:15 (V:Sc:C) as raw material, $V_xSc_{3-x}N@C_{80}$ (x = 1, 2) were synthesized by a modified Krätschmer-Huffman DC arc-discharge method with addition of 20 mbar N_2 and 400 mbar He. The soot was collected and Soxhlet-extracted by CS_2 for 24 h, then the resulting brown-yellow solution was distilled to remove CS_2 and immediately redissolved in toluene for HPLC isolation. $V_xSc_{3-x}N@C_{80}$ (x = 1, 2) were isolated by three-step HPLC (LC-9104, Japan Analytical Industry) as described in details in Supporting Information S4. The purity of isolated products was checked by LD-TOF MS analysis (Autoflex speed TOF/TOF, Bruker Daltonics Inc., Germany).

Spectroscopic and Electrochemical Study. UV−vis−NIR spectra of $V_xSc_{3-x}N@C_{80}$ (x = 1, 2) dissolved in toluene or CS_2 were recorded on a UV−vis−NIR 3600 spectrometer (Shimadzu, Japan) using quartz cell of 1 mm layer thickness and 1 nm resolution. ESR spectra were measured in toluene using a JES-FA200 FT-EPR X-band spectrometer (JEOL, Japan). The ^{13}C NMR spectroscopic study was performed in an Advance AV 400 spectrometer (Bruker, Germany) at room temperature in carbon disulfide with acetone-d_6 as an external lock.

Electrochemical study of $V_xSc_{3-x}N@C_{80}$ (x = 1, 2) was performed in o-dichlorobenzene (o-DCB, anhydrous, 99%, Aldrich). The supporting electrolyte was tetrabutylamonium hexafluorophosphate ($TBAPF_6$, puriss. electrochemical grade, Fluka) which was dried under pressure at 340 K for 24 h and stored in glovebox prior to use. Cyclic voltammogram experiments were performed with a CHI 660D potentiostat (CHI Instrument, USA) at room temperature in a glovebox. A standard three-electrode arrangement of a platinum (Pt) wire as working electrode, a platinum coil as counter electrode, and a silver wire as a pseudoreference electrode was used. In a comparison

DOI: 10.1021/jacs.5b10115
J. Am. Chem. Soc. 2016, 138, 207−214

experiment, ferrocene (Fc) was added as the internal standard and all potentials are referred to Fc/Fc^+ couple.

Details of Computations. Our calculation are performed using density functional theory (DFT) as implemented in the DMol[3] package based on the linear combination of the atomic orbital-molecular orbital. The atomic orbitals are represented by a double-numeric quality basis set with polarization functions (DNP), which are comparable to Gaussian 6-31G** sets. The exchange correlation interactions are described by the Perdew−Burke−Ernzerhof generalized gradient approximation (GGA). All atomic positions are fully relaxed at the GGA level without symmetry restriction until the atomic forces are smaller than 10^{-5} Hartree.[33]

X-ray Crystallographic Study. Crystal growths for $VSc_2N@C_{80}\cdot Ni^{II}(OEP)\cdot 1.66C_6H_6\cdot CHCl_3$ and $V_2ScN@C_{80}\cdot Ni^{II}(OEP)\cdot 2C_6H_6$ were accomplished by layering 1 mL of saturated benzene solution of $V_xSc_{3-x}N@C_{80}$ (x = 1, 2) over a solution of 2 mL of saturated chloroform (for $VSc_2N@C_{80}$) or benzene (for $V_2ScN@C_{80}$) solution of $Ni^{II}(OEP)$ respectively. After the two solutions diffused together over a period of about one month, small black crystals suitable for X-ray crystallographic study formed upon a slow evaporation of benzene. X-ray data collection for the crystal of $VSc_2N@C_{80}\cdot Ni^{II}(OEP)\cdot 1.66C_6H_6\cdot 0.33CHCl_3$ ($0.15 \times 0.17 \times 0.22$ mm^3) was carried out at 100 K on a Gemini S Ultra diffractometer (Oxford diffraction Ltd., UK) with a 92 mm Sapphire CCD image plate detector. $VSc_2N@C_{80}\cdot Ni^{II}(OEP)\cdot 1.66C_6H_6\cdot CHCl_3$ crystallizes in the monoclinic space group $C2/m$; a = 25.273(5) Å, b = 15.103(5) Å, c = 19.695(5) Å, V = 7486(3) Å^3, Z = 4. X-ray data collection for the crystal of $V_2ScN@C_{80}\cdot Ni^{II}(OEP)\cdot 2C_6H_6$ ($0.11 \times 0.21 \times 0.26$ mm^3) was carried out at 100 K on an Agilent Supernova diffractometer (Agilent Technologies, U.S.A.) with a Cu radiation (λ = 1.54178 Å). $V_2ScN@C_{80}\cdot Ni^{II}(OEP)\cdot 2C_6H_6$ crystallizes in the monoclinic space group $C2/m$; a = 25.2821(15) Å, b = 15.1254(10) Å, c = 19.7824(16) Å, V = 7538.1(9) Å^3, Z = 4. A numerical absorption correction utilizing equivalents was employed. The structure was solved by direct methods and refined using all data (based on F^2) by SHELXL 2014,[45] and the details on their crystal and structure data are summarized in Supporting Information Tables S2 and S3. These data can be obtained free of charge from The Cambridge Crystallographic Data Centre with CCDC Nos. 930733 and 1420968.

■ ASSOCIATED CONTENT

Supporting Information

The Supporting Information is available free of charge on the ACS Publications website at DOI: 10.1021/jacs.5b10115.

HPLC profiles of extract mixtures obtained under different conditions, LD-TOF mass spectra, Isolation of $V_xSc_{3-x}N@C_{80}$ (x = 1, 2), X-ray crystallographic data of $V_xSc_{3-x}N@C_{80}$ (x = 1, 2), UV−vis−NIR and ESR spectra of $V_xSc_{3-x}N@C_{80}$ (x = 1, 2), DFT calculated spin densities of $V_xSc_{3-x}N@C_{80}$ (x = 1, 2), and cyclic voltammograms of $V_xSc_{3-x}N@C_{80}$ (x = 1, 2) in different scanning regions. (PDF)

X-ray crystallographic file. (CIF)

X-ray crystallographic file. (CIF)

■ AUTHOR INFORMATION

Corresponding Author

*sfyang@ustc.edu.cn

Notes

The authors declare no competing financial interest.

■ ACKNOWLEDGMENTS

This work was partially supported by the National Natural Science Foundation of China (Nos. 21132007, 21371164) [to SFY]. Q. L. thanks the National Natural Science Foundation of China (No. 21473168) and the National Basic Research Program of China (No. 2014CB921101).

■ REFERENCES

(1) Popov, A. A.; Yang, S. F.; Dunsch, L. *Chem. Rev.* **2013**, *113*, 5989.
(2) Tan, Y. Z.; Xie, S. Y.; Huang, R. B.; Zheng, L. S. *Nat. Chem.* **2009**, *1*, 450.
(3) Lu, X.; Feng, L.; Akasaka, T.; Nagase, S. *Chem. Soc. Rev.* **2012**, *41*, 7723.
(4) Wang, T. S.; Wang, C. R. *Acc. Chem. Res.* **2014**, *47*, 450.
(5) Rodríguez-Fortea, A.; Balch, A. L.; Poblet, J. M. *Chem. Soc. Rev.* **2011**, *40*, 3551.
(6) Chaur, M. N.; Melin, F.; Ortiz, A. L.; Echegoyen, L. *Angew. Chem., Int. Ed.* **2009**, *48*, 7514.
(7) Zhang, J. Y.; Stevenson, S.; Dorn, H. C. *Acc. Chem. Res.* **2013**, *46*, 1548.
(8) Yang, S. F.; Liu, F. P.; Chen, C. B.; Jiao, M. Z.; Wei, T. *Chem. Commun.* **2011**, *47*, 11822.
(9) Yang, S. F.; Wang, C. R. *Endohedral Fullerenes: From Fundamentals to Applications*; World Scientific Publishing Co. Pte. Ltd.: Singapore, 2014.
(10) Chaur, M. N.; Valencia, R.; Rodríguez-Fortea, A.; Poblet, J. M.; Echegoyen, L. *Angew. Chem., Int. Ed.* **2009**, *48*, 1425.
(11) Chai, Y.; Guo, T.; Jin, C.; Haufler, R. E.; Chibante, L. P. F.; Fure, J.; Wang, L.; Alford, G. M.; Smalley, R. E. *J. Phys. Chem.* **1991**, *95*, 7564.
(12) Shinohara, H. *Rep. Prog. Phys.* **2000**, *63*, 843.
(13) Wan, S. M.; Zhang, H. W. *J. Am. Chem. Soc.* **1998**, *120*, 6806.
(14) Reich, A.; Panthöfer, M.; Modrow, H.; Wedig, U.; Jansen, M. *J. Am. Chem. Soc.* **2004**, *126*, 14428.
(15) Aoyagi, S.; Nishibori, E. J.; Sawa, H.; Sugimoto, K.; Takata, M.; Miyata, Y.; Kitaura, R.; Shinohara, H.; Okada, H.; Sakai, T.; Ono, Y.; Kawwachi, K.; Yokoo, K.; Ono, S.; Omote, K.; Kasama, Y.; Ishikawa, S.; Komuro, T.; Tobita, H. *Nat. Chem.* **2010**, *2*, 678.
(16) Wan, Z.; Christian, J. F.; Basir, Y.; Anderson, S. *J. Chem. Phys.* **1993**, *99*, 5858.
(17) Hino, S.; Kato, M.; Yoshimura, D.; Moribe, H.; Umemoto, H.; Ito, Y.; Sugai, T.; Shinohara, H.; Otani, M.; Yoshimoto, Y.; Okada, S. *Phys. Rev. B: Condens. Matter Mater. Phys.* **2007**, *75*, 125418.
(18) Yang, S. F.; Chen, C. B.; Popov, A. A.; Zhang, W. F.; Liu, F. P.; Dunsch, L. *Chem. Commun.* **2009**, 6391.
(19) Dunk, P. W.; Kaiser, N. K.; Mulet-Gas, M.; Rodriguez-Fortea, A.; Pblet, J. M.; Shinohara, H.; Hendrickson, C. L.; Marshall, A. G.; Kroto, H. *J. Am. Chem. Soc.* **2012**, *134*, 9380.
(20) Dunsch, L.; Yang, S. F. *Small* **2007**, *3*, 1298.
(21) Shannon, R. D. *Acta Crystallogr., Sect. A: Cryst. Phys., Diffr., Theor. Gen. Crystallogr.* **1976**, *A32*, 751.
(22) Stevenson, S.; Rice, G.; Glass, T.; Harich, K.; Cromer, F.; Jordan, M. R.; Craft, J.; Hadju, E.; Bible, R.; Olmstead, M. M.; Martra, K.; Fisher, A. J.; Balch, A. L.; Dorn, H. C. *Nature* **1999**, *401*, 55.
(23) Yang, S. F.; Liu, F. P.; Chen, C. B.; Zhang, W. F. *Prog. Chem.* **2010**, *22*, 1869.
(24) Popov, A. A.; Chen, C. B.; Yang, S. F.; Lipps, F.; Dunsch, L. *ACS Nano* **2010**, *4*, 4857.
(25) Chen, C. B.; Liu, F. P.; Li, S. J.; Wang, N.; Popov, A.; Jiao, M. Z.; Wei, T.; Li, Q. X.; Dunsch, L.; Yang, S. F. *Inorg. Chem.* **2012**, *51*, 3039.
(26) Chen, N.; Fan, L. Z.; Tan, K.; Wu, Y. Q.; Shu, C. Y.; Lu, X.; Wang, C. R. *J. Phys. Chem. C* **2007**, *111*, 11823.
(27) Yang, S. F.; Popov, A. A.; Chen, C.; Dunsch, L. *J. Phys. Chem. C* **2009**, *113*, 7616.
(28) Yang, S. F.; Popov, A.; Kalbac, M.; Dunsch, L. *Chem. - Eur. J.* **2008**, *14*, 2084.
(29) Wei, T.; Liu, F. P.; Wang, S.; Zhu, X. J.; Popov, A. A.; Yang, S. F. *Chem. - Eur. J.* **2015**, *21*, 5750.
(30) Zhang, Y.; Popov, A. A.; Schiemenz, S.; Dunsch, L. *Chem. - Eur. J.* **2010**, *18*, 9691.
(31) Wei, T.; Wang, S.; Liu, F. P.; Tan, Y. Z.; Zhu, X. J.; Xie, S. Y.; Yang, S. F. *J. Am. Chem. Soc.* **2015**, *137*, 3119.

DOI: 10.1021/jacs.5b10115
J. Am. Chem. Soc. 2016, 138, 207−214

(32) Yang, H.; Jin, H.; Wang, X.; Liu, Z.; Yu, M.; Zhao, F.; Mercado, B. Q.; Olmstead, M. M.; Balch, A. L. *J. Am. Chem. Soc.* **2012**, *134*, 14127.
(33) Yang, S.; Chen, C.; Liu, F.; Xie, Y.; Li, F.; Jiao, M.; Suzuki, M.; Wei, T.; Wang, S.; Chen, Z.; Lu, X.; Akasaka, T. *Sci. Rep.* **2013**, *3*, 1487.
(34) Liu, F. P.; Wang, S.; Guan, J.; Wei, T.; Zeng, M. X.; Yang, S. F. *Inorg. Chem.* **2014**, *53*, 5201.
(35) Svitova, A. L.; Ghiassi, K. B.; Schlesier, C.; Junghans, K.; Zhang, Y.; Olmstead, M. M.; Balch, A. L.; Dunsch, L.; Popov, A. A. *Nat. Commun.* **2014**, *5*, 3568.
(36) Chen, C. H.; Ghiassi, K. B.; Ceron, M. R.; Guerrero-Ayala, M. A.; Echegoyen, L.; Olmstead, M. M.; Balch, A. L. *J. Am. Chem. Soc.* **2015**, *137*, 10116.
(37) Zhang, Y.; Ghiassi, K. B.; Deng, Q.; Samoylova, N. A.; Olmstead, M. M.; Balch, A. L.; Popov, A. A. *Angew. Chem., Int. Ed.* **2014**, *54*, 495.
(38) Yang, S. F.; Troyanov, S. I.; Popov, A. A.; Krause, M.; Dunsch, L. *J. Am. Chem. Soc.* **2006**, *128*, 16733.
(39) Olmstead, M. M.; de Bettencourt-Dias, A.; Duchamp, J. C.; Stevenson, S.; Dorn, H. C.; Balch, A. L. *J. Am. Chem. Soc.* **2000**, *122*, 12220.
(40) Stevenson, S.; Chancellor, C. J.; Lee, H. M.; Olmstead, M. M.; Balch, A. L. *Inorg. Chem.* **2008**, *47*, 1420.
(41) Stevenson, S.; Rose, C. B.; Maslenikova, J. S.; Villarreal, J. R.; Mackey, M. A.; Mercado, B. Q.; Chen, K.; Olmstead, M. M.; Balch, A. L. *Inorg. Chem.* **2012**, *51*, 13096.
(42) Wang, X. L.; Zuo, T. M.; Olmstead, M. M.; Duchamp, J. C.; Glass, T. E.; Cromer, F.; Balch, A. L.; Dorn, H. C. *J. Am. Chem. Soc.* **2006**, *128*, 8884.
(43) Stevenson, S.; Phillips, J. P.; Reid, J. E.; Olmstead, M. M.; Rath, S. P.; Balch, A. L. *Chem. Commun.* **2004**, 2814.
(44) Stevenson, S.; Lee, H. M.; Olmstead, M. M.; Kozikowski, C.; Stevenson, P.; Balch, A. L. *Chem. - Eur. J.* **2002**, *8*, 4528.
(45) Sheldrick, G. *Acta Crystallogr.* **2015**, *C71*, 3.

DOI: 10.1021/jacs.5b10115
J. Am. Chem. Soc. 2016, 138, 207−214